12 Light scattering methods

Dr. Theodore V. Vorburger, Dr. Richard Silver

Precision Engineering Division, National Institute of Standards and Technology

100 Bureau Drive, Stop 8212

Gaithersburg, MD 20899, USA

Dr. Rainer Brodmann, Boris Brodmann

OptoSurf GmbH

Nobelstrasse 9-13, 76275 Ettlingen

Germany

Dr. Jörg Seewig

Technische Universitat Kaiserslautern

Gottlieb-Daimler-Strasse

67663 Kaiserslautern

Germany

Abstract Light scattering belongs to a class of techniques known as area-integrating methods for measuring surface texture. Rather than relying on coordinate measurements of surface points, these methods probe an area of the surface altogether and yield parameters that are characteristic of the texture of the area as a whole. The specular beam intensity, the angle resolved scatter, and the angle integrated scatter are examples of measurands from light scattering that can yield useful parameters of the surface texture. Uses of light scatter for inspecting the surfaces of mechanical and optical components as well as surfaces produced in semiconductor manufacturing are primarily reviewed here. Several documentary standards describing best practices are also briefly reviewed.

12.1 Introduction

Since the beginnings of optical technology in ancient times (Flinn 2010), people have understood that smooth surfaces are mirror-like and that rough surfaces scatter light in many directions. This phenomenon of light scattering has been used since the early 1960s (Bennett and Porteus 1961, Bennett and Mattsson 1989, Griffiths et al. 1994) to help quantify surface roughness. The theory is well founded and has been extensively developed, and the designs of light scattering instrumentation have greatly varied. In this chapter the theory of light scattering from surfaces will be briefly outlined, and a number of different ways in which light scatter can be used to measure surface roughness will be described.

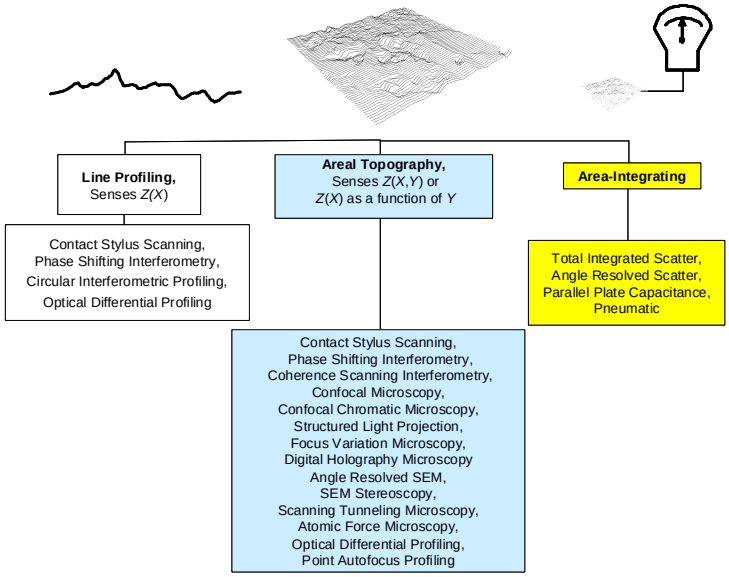

Fig. 12.1 A classification of surface texture measurement methods with examples (Vorburger et al. 2007, ISO 2010a)

As indicated in Chap. 1, methods for measuring rough surfaces may be classified into three types (Fig. 12.1): line profiling, areal topography and area-integrating (Vorburger et al. 2007, ISO 2010a). Line profiling and areal topography methods are coordinate based and are similar to one another. Area-integrating methods are quite different. These methods sense an area of the surface as a whole and provide a measure of the overall surface roughness of that area, perhaps even with a single measured parameter. The most widely used of these methods are based on light scattering. We illustrate two important types of light scatter methods: *angle resolved scatter* (Fig. 12.2), where the light scattered in different direc-

tions is measured and analyzed, and *total integrated scatter* (Fig. 12.3), where essentially all of the light that is not specularly reflected is captured.

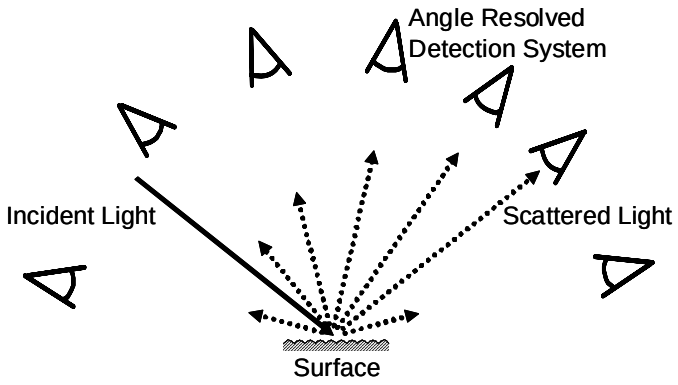

Figure 12.2 Schematic diagram of light scattering from a rough surface and an angle resolved detection system consisting here of a number of detectors. Alternatively, the system could have a moving detector.

When a beam of laser light is incident on a smooth surface most of the reflected light travels in the specular direction such that the angle of reflection equals the angle of incidence, as suggested by Fig. 12.2. As the surface roughness increases, more light is scattered into different directions and the reflected specular beam loses intensity. The theory (for example, Beckmann and Spizzichino 1987) that describes these phenomena comes from electromagnetism. Specifically, the theory describes the behavior of the electric and magnetic fields that compose propagating beams of light and their behavior when boundaries, such as reflecting surfaces, are encountered in the medium of propagation. The focus of this chapter is on the specular beam and the overall angle resolved scatter distribution. Laser speckle effects (Asakura 1978) and changes in polarization upon reflection (Azzam and Bashara 1977) are also sensitive to surface roughness, but such phenomena will not be discussed here.

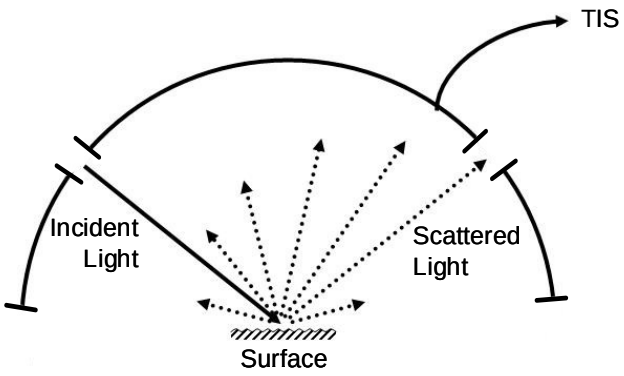

Fig. 12.3 Schematic diagram of light scattering from a rough surface and a device for collecting the total integrated scattered light (TIS)

12.2 Basic theory

A relatively simple theory for an electromagnetic boundary problem is illustrated in Fig. 12.4. The light is incident from the upper left with direction vector $\vec{\mathbf{K}}_i$, and it illuminates an area of an undulating (rough) surface. To simplify the geometrical arguments here, it is assumed that the surface is smooth along the *y*-direction and that the light is incident in the *x*-*z* plane as shown. The reflected light is scattered into a wide range of angles θ_s in the circle above the surface. If the surface is only moderately rough most of the reflected light proceeds in the specular direction associated with reflection from the mean plane of the surface. For the 2D schematic diagram shown here, the specular direction is such that $\theta_{spec} = \theta_i$. In addition, if the surface is transparent, some of the light will travel through the material, but that situation will not be discussed here, and only the reflected light will be described.

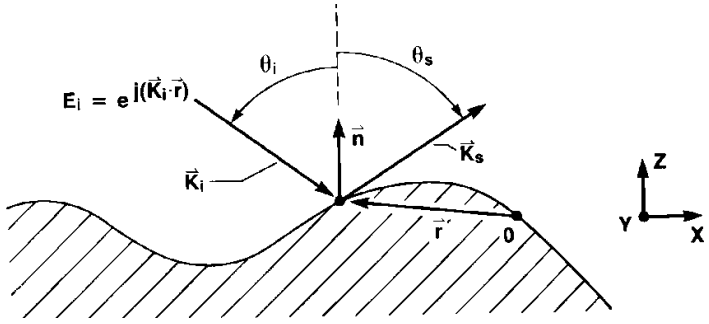

Fig. 12.4 Schematic diagram of key quantities associated with the electromagnetic boundary value problem describing light scattering from a rough surface. The incoming plane wave has direction vector $\vec{\mathbf{K}}_i$ with polar angle θ_i with respect to the normal $\vec{\mathbf{n}}$ of the mean plane of the surface. The theory aims to calculate the electric field in any direction θ_s from knowledge of the incident electric field $\mathbf{E}_i$ and the surface roughness $z(x)$.

The boundary value problem that models the light-surface interaction may be approximated and described by the following equation if the surface is highly reflecting and has moderate slopes (Beckmann and Spizzichino 1987)

$$E(\theta_s) = F(\theta_i, \theta_s) \int_0^L \exp(j\,\vec{\mathbf{V}} \bullet \vec{\mathbf{r}})\, \mathrm{d}x \tag{12.1}$$

where $E(\theta_s)$ is the electric field of the scattered light, expressed here as a scalar, F contains a known trigonometric function of the angles and is also proportional to the incident electric field, 0 to L indicates the extent of the illuminated region, j is equal to $(-1)^{1/2}$, $\vec{\mathbf{V}} = \vec{\mathbf{K}}_i - \vec{\mathbf{K}}_s$, that is, $\vec{\mathbf{V}}$ is the vector difference between the wave vector of the incident light traveling in the direction θ_i and the wave vector of the scattered light for a particular direction θ_s, the magnitude of both wave vectors is $2\pi/\lambda$, where λ is the wavelength of the incident light, and $\vec{\mathbf{r}}$ $(= x\hat{\mathbf{e}}_x + z(x)\hat{\mathbf{e}}_z)$ is the vector from the coordinate origin (O) to the points on the illuminated surface over which the integration is taken.

Furthermore, the dot product $\vec{\mathbf{V}} \bullet \vec{\mathbf{r}}$ contains the mathematical description of the surface profile (x, $z(x)$), and the flux density of the scattered light is proportional to $|E(\theta_s)|^2$ and is termed $I(\theta_s)$. Therefore, equation (12.1) indicates how the

flux density of scattered light may be related to the surface roughness profile of the illuminated region and vice versa.

Under a number of conditions, including especially the assumption of a Gaussian height distribution function of surface heights, equation (12.1) leads to a relationship (Beckmann and Spizzichino 1987) for the magnitude P_{spec} of the light flux reflected into the specular direction given by

$$P_{spec} = P_0 \exp\{-[4\pi(Rq)\cos\theta_i / \lambda]^2\}, \tag{12.2}$$

where P_0 is the total reflected flux, and Rq is the root mean square (RMS) roughness of the surface. For now, equation (12.1) for the electric field along a non-specular direction θ_s will be examined. A useful simplification results if the surface roughness is much smaller than the wavelength of the incident light. Then the exponential term $\exp(j\vec{\mathbf{V}} \bullet \vec{\mathbf{r}})$ in equation (12.1) may be approximated by its first order equivalent $\exp(jV_x x)[1 + jV_z z]$. The flux density $I(\theta_s)$ as a function of scatter angle may then be described approximately by the following (Elson and Bennett 1979, Church et al. 1979):

$$I(\theta_s) = [F_1(\theta_s)/\lambda^4]\left|\int_0^L \exp(jV_x x)\, z(x)\, dx\right|^2, \tag{12.3}$$

where F_1 is another known trigonometric function. The flux density in a non-specular direction is still a function of the roughness profile; however, the integral on the right hand side of equation (12.3) is a close approximation to the power spectral density function (PSD) of the surface profile.

Equations (12.2) and (12.3) give two approaches to quantify the surface roughness in terms of scattered light. Equation (12.2) can be inverted to yield

$$Rq = (\lambda / 4\pi\cos\theta_i)\,[\ln(P_0 / P_{spec})]^{1/2}, \tag{12.4}$$

which indicates that the RMS roughness Rq can be determined from measurement of the light flux scattered into the specular direction (Bennett and Porteus 1961). This relationship is especially useful when the surface is moderately rough and the specular intensity is decreasing exponentially fast with increasing roughness, so that an accurate determination of roughness can be made from a measurement of the specular beam. Equation (12.2) is not at all useful when the surface is so rough that the specular beam is so small as to be un-measurable. It is also not useful when the surface is very smooth and the specular intensity comprises nearly all the reflected light. For smooth surfaces it is more useful to measure the small fraction

of integrated scattered light ($P_{\text{scat}} = P_0 - P_{\text{spec}}$) and use the approximate relationship (Davies 1954),

$$Rq = (\lambda / 4\pi \cos\theta_i)(P_{\text{scat}} / P_{\text{spec}})^{1/2}. \tag{12.5}$$

This is the principle of the technique of total integrated scatter (TIS) (Bennett and Mattsson 1989, Stover 1995), an approach for which a documentary standard was developed (SEMI MF 2009).

For smooth surfaces the angular distribution of scattered light is closely related by equation (12.3) to the PSD of the surface, which describes the decomposition of the surface profile into its component spatial frequencies f (= 1/d), where d is a component spatial wavelength. So a measurement of the angular distribution of scattered light can yield the PSD. The spatial wavelength d is related to the scattering angle by

$$2\pi / d = V_x = (2\pi / \lambda)\ (\sin\theta_s - \sin\theta_i), \tag{12.6}$$

which reduces to the relationship

$$\sin\theta_s = \sin\theta_i + \lambda / d. \tag{12.7}$$

Equation (12.7) shows the mapping between the spatial frequency (1/d) and the scattering angle θ_s. Small surface spatial wavelengths d scatter the light into large angles θ_s with respect to the specular direction θ_{spec} (= θ_i), and large spatial wavelengths of the surface scatter light into angles very close to the specular direction.

Equations (12.3) and (12.7) have been used a great deal by opticists (Elson and Bennett 1979, Church et al. 1979, Stover 1988) to describe and measure the quality of optical surfaces, where the RMS roughness is much smaller than the wavelengths of visible light. For slightly rougher surfaces these relationships become more complex. Equation (12.7), in particular, is generalized to

$$\sin\theta_s = \sin\theta_i + m\lambda / d, \tag{12.8}$$

where m is an integer (0, ±1, ±2, …). Equation (12.8) is the diffraction equation (Beckmann and Spizzichino 1987), which is useful to describe the scattered light

from periodic gratings of any amplitude and any combination of spatial wavelengths. A particular spatial wavelength d scatters light into specific directions given by different diffraction orders m.

For ordinary rough surfaces, with a continuum of spatial wavelengths and heights, equation (12.3) is no longer valid, but for a limited range of slightly rough surfaces, it is still possible to obtain the surface autocorrelation function from a measurement of the angle resolved light scatter (Chandley 1976).

One more relationship is important. Given the assumption that the surface has moderate slopes, it has been shown (for example Rakels 1989) that the RMS width of the distribution of scattered light (Γ) is proportional to the RMS width of the distribution of slopes on the surface Rdq:

$$Rdq = 0.5\ \Gamma. \tag{12.9}$$

where, say, both quantities are expressed in radians or as tangents. Therefore, the RMS surface slope can be obtained from measurement of the RMS width of the scattered light (Cao et al. 1991). This relationship is derivable both from the theory of physical optics and from geometrical optics using a facet model to describe the scattered light.

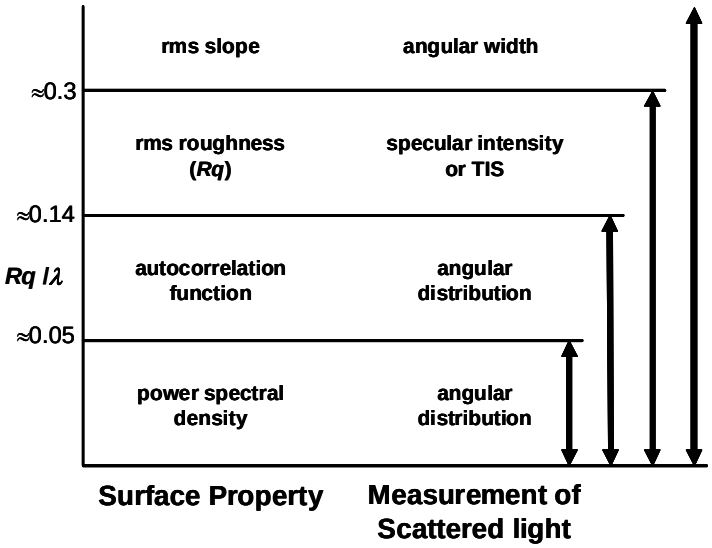

Fig. 12.5 Schematic diagram showing regimes of roughness for which measurable properties of the scattered light are paired with surface parameters or functions that may be derived from them (Vorburger et al. 1993)

Now the limitations of these relationships in terms of measurable amplitude and spatial wavelength will be investigated. Figure 12.5 (Vorburger et al. 1993) shows approximate limitations in amplitude for the validity of the four approaches described above. These limitations are expressed in terms of the ratio of RMS roughness (*Rq*) to the wavelength λ of the incident light. Note that the boundaries shown here are only approximate.

For the smoothest surfaces the angle resolved scatter (ARS) distribution directly yields the surface PSD. A criterion for the upper limit of $Rq/\lambda \approx 0.05$ was proposed elsewhere (Vorburger et al. 1993). If the surface is slightly rougher, one can still measure the angle resolved scatter distribution and calculate the autocorrelation function (Chandley 1976). At approximately $Rq/\lambda = 0.14$, this operation is no longer mathematically feasible (Marx et al. 1993).

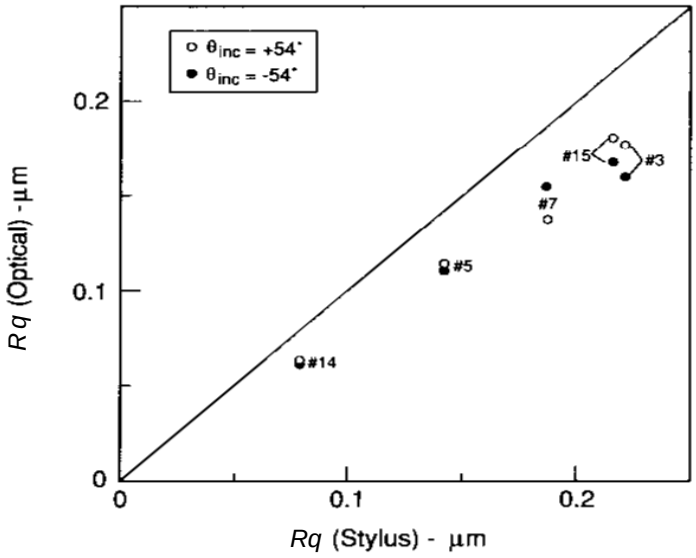

Fig. 12.6 Comparison of *Rq* values calculated from optical scattering and from stylus profiles for a set of five hand lapped surfaces. The incident light for this study was ± 54° from the surface normal by turns. The diagonal line indicates a slope of unity (Marx and Vorburger 1990)

Rq can still be calculated so long as there is a measurable specular spot (that is, the surface still appears a little glossy), but the approximate limitation there is $Rq/\lambda \approx 0.3$, and only if the light is incident at a high angle θ_i where $\cos\theta_i$ is small (see equation (12.2)). An example is shown in Fig. 12.6 (Marx and Vorburger 1990), where the *Rq* values calculated from measurement of the specular beam using equation (12.4) are plotted versus the *Rq* values obtained from profiles meas-

ured with a stylus instrument for a set of five hand lapped surfaces of differing roughness. The correlation coefficient between the two sets of *Rq* values is 0.986. The optical values are systematically smaller than the stylus values, likely because the spatial bandwidth limits of the two instruments are different.

Finally, the width of the angle resolved scatter can be used as an estimator of the RMS slope of the surface using the relationship derivable both from physical optics and geometrical optics and represented here by equation (12.9).

As with surface profiling instruments, there are limitations in the surface spatial wavelengths (*d*) that may be assessed by light scattering (Church 1979). The shortest measurable spatial wavelengths are determined, in light of the diffraction equation (12.8), by the largest angles of scattered light that can be collected by the instrument. For normal incidence light, the limit is $d = \lambda$, assuming that the instrument can capture light scattered right at the horizon. Conversely, long spatial wavelengths scatter light into small angles very close to the specular beam, so the long wavelength limit is determined in principle by the size of the specular spot in the plane of detection or by apertures in the instrument used to detect the specular beam, or conversely, by apertures allowing the specular beam to pass through the instrument. For smooth surfaces, where the index *m* only takes the value of one and higher orders are insignificant, this limit is easily determined by the diffraction equation with $m = \pm 1$. For example, if the specular spot has a diameter of 1 mm at the detector and the detector is located at a radius (*R*) of 100 mm from the sample, then the angular width of the specular spot ($\Delta\theta$) is approximately 0.005 rad. Assuming that the wavelength of the incident light is 0.6 μm and is normally incident on the surface, the largest measurable spatial wavelength is approximately given by

$$d \approx \lambda / \sin(\Delta\theta) = 0.6\ \mu\text{m} / \sin(0.005\ \text{rad}) = 120\ \ \mu\text{m}. \qquad (12.10)$$

For moderately rough surfaces higher values of *m* become significant in equation (12.8), and the limit is not so clear cut. In principle, rough surfaces with very long spatial wavelengths can produce measurable scattered light at high orders *m* outside the specular spot. Therefore, long spatial wavelengths, whose first order scattered light may lie inside the specular spot and remain undetectable, may also have sufficient amplitude to produce higher scattering orders that lie outside the specular spot and are detected. Hence the long spatial wavelength cutoff is difficult to characterize for rough surfaces.

12.3 Instrumentation and case studies

12.3.1 Early developments

From the 1960s, a number of light scatter instruments were custom developed by manufacturers of optical surfaces and by surface metrology researchers but were not commercialized. One notable example is the goniometric optical scatter instrument (GOSI) developed at NIST (Germer and Asmail 1997) for calibrated measurements of scattered light flux. However, several companies have also produced light scatter products*. Commercial glossmeters, for example, are fairly common, and physical standards for glossmeters have been developed (Nadal and Thompson 2000).

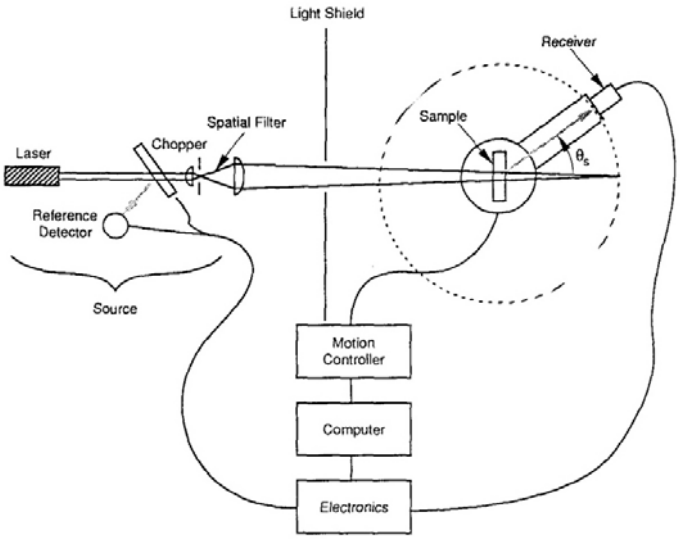

Fig. 12.7 Schematic diagram of an apparatus to measure angle resolved scattering (Stover 1995, reprinted with permission,)

* Certain commercial equipment, instruments or materials are identified in this paper to specify adequately certain experimental procedures. Such identification does not imply recommendation or endorsement by the National Institute of Standards and Technology, nor does it imply that the materials or equipment identified are necessarily the best available for the purpose.

Several other examples of commercial instruments intended for quantitative measurement of surface texture parameters are cited here. Stover et al. have developed a line of angle resolved scatterometers intended mainly for the study of smooth optical and semiconductor surfaces. A typical scatterometer design (Stover 1995) is shown in Fig. 12.7.

To assess the quality of optically smooth surfaces, these instruments operate over a wide dynamic range of scattering angles and flux levels. These capabilities are important for the study of very smooth surfaces, such as laser gyro mirrors, where small amounts of light scatter affect the function of the device and need to be specified. Typically, high quality scatterometers can detect scattered light flux ten orders of magnitude smaller than the specular beam flux as well as light scattered within 0.1° of the specular beam by long spatial wavelengths of the surface.

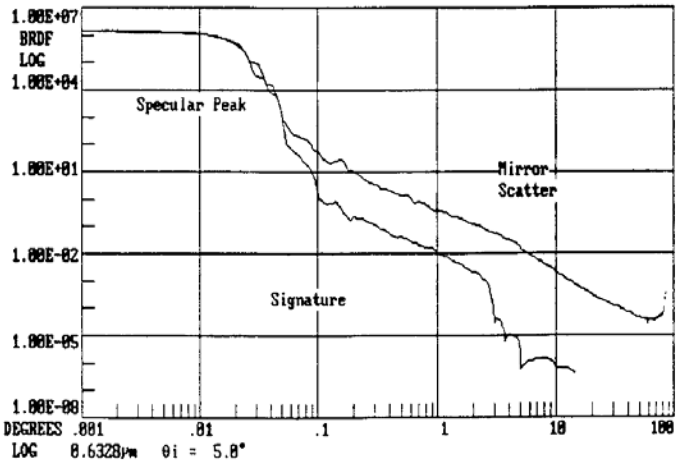

Fig. 12.8 BRDF from a molybdenum mirror measured as a function of scattering angle. The scale is logarithmic along both axes. Separation from the instrument signature and meaningful data are obtained beyond about 0.1° (Stover 1995, reprinted with permission)

Figure 12.8 shows a typical measured angle resolved scattering distribution function, in this case for a molybdenum mirror (Stover 1995). The distribution is expressed as the bidirectional reflectance distribution function (BRDF), a quantity that will be discussed further in Sect. 12.4.2. Note that both the BRDF and the scatter angle are plotted logarithmically. The upper curve is the measured BRDF as a function of angle in the plane of incidence. The lower curve is the instrument signature, which is the measured function when there is no sample in place. The instrument signature represents scattering from various surfaces in the instrument and along the air path. Figure 12.8 shows BRDF measurements over roughly twelve orders of magnitude and shows good separation between the mirror scatter,

the quantity to be measured, and the instrument signature to within 0.1° of the specular peak.

A portable commercial instrument (Fig. 12.9), developed by Brodmann et al. (Brodmann et al. 1985, Brodmann and Allgäuer 1988), was mainly intended for the study of moderately rough surfaces in a manufacturing environment and even during the machining process. The angle of incidence is near normal. Because a single housing contains both the light source and the detection system, the instrument is useful (Zimmerman et al. 1988) for automated alignment with respect to the surface being measured, an important function for quality control of parts during manufacture.

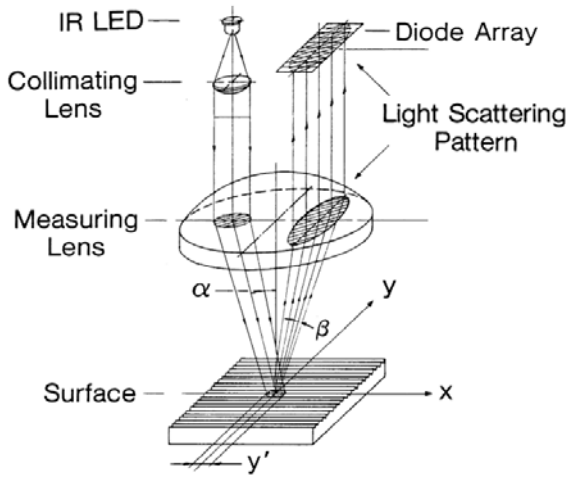

Fig. 12.9 Schematic diagram of an optical scatterometer. IR LED stands for infrared light emitting diode (Brodmann and Allgäuer 1988, reprinted with permission,)

Subsequently, Kiely et al. (Kiely 1991) experimentally showed for a set of hand lapped components the expected correlation between the RMS width of the light scattering distribution measured with the instrument and the RMS slope of the surface as measured with a stylus instrument.

A different commercial instrument for control of surfaces in manufacturing environments was developed by Valliant (Valliant et al. 2000) and is shown in Fig. 12.10. Once again both the source and the receiver components are located in a single housing. The angle of incidence is approximately 75° here. Mechanisms for monitoring and compensating for vibrations during measurements in the manufacturing operation make integration of the scatterometer technology into the plant environment possible. The instrument shown in Fig. 12.10 is one of several having different sizes and degrees of portability.

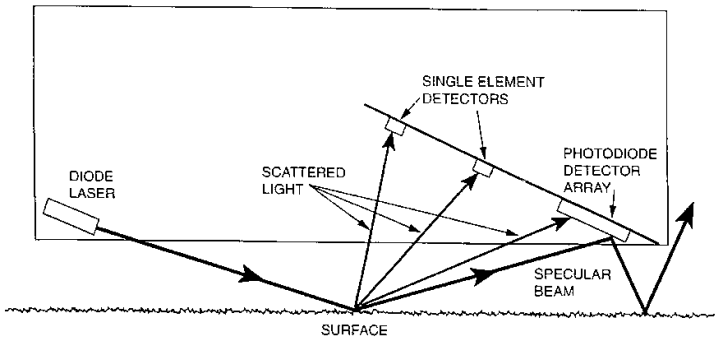

Fig. 12.10 Schematic diagram of Lasercheck optical scatterometer (Valliant et al. 2000, reprinted with permission).

12.3.2 Recent developments in instrumentation for mechanical engineering manufacture

The commercial light scattering technologies of Brodmann et al. (1988) and Valliant (2000) have been developed further for in-line measurement on the shop floor (Brodmann et al. 2009, Optosurf 2010a, Schmitt Industries 2010). The sensor recently developed by Brodmann et al. has high dynamic range (16 bit), a measurement time of 0.5 ms, and software packages for roughness and form analysis. Following a recent guideline developed for scattered light measurement (Sect. 12.4.5) a roughness parameter called Aq is calculated, which describes the variance in angle of the scattered light distribution recorded by the sensor. The focus of the applications is the assessment of roughness and form of fine machined mechanical surfaces including automotive parts, such as finished bearings of crankshafts (Fig. 12.11), piston bolts, steering gearing components and gear shafts.

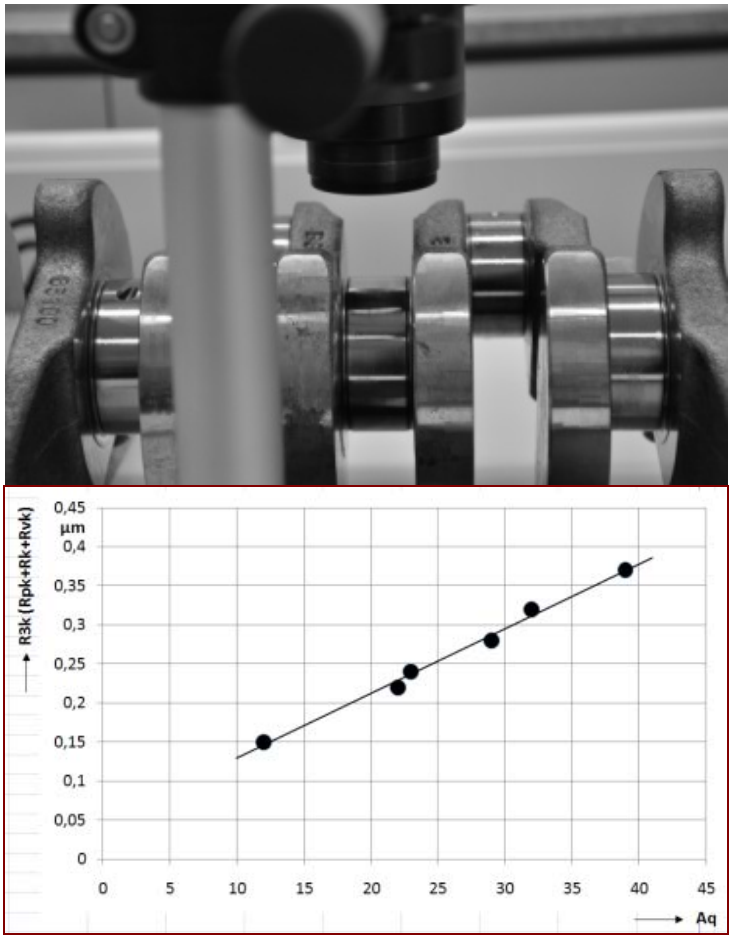

Fig 12.11 Scattered light sensor shown measuring the bearings of crankshafts (top). The scattered light roughness value *Aq* correlates with the *R3k*-roughness parameter (bottom), which equals *Rpk* + *Rk* + *Rvk* (ISO 1996), courtesy of T. Hercke, Daimler AG (Optosurf 2010b)

Scattered light sensors can be used in an oil-vapour environment close to the manufacturing process. Based on the specific capability of the scattered light method to measure polished surfaces, scatterometry has also found application in biomedical device manufacturing for 100 % measurement of artificial femoral heads. The sensor may be used with two precision rotary stages. One stage rotates the sample and the other pivots the sensor across the entire surface. Such a system is shown in Fig. 12.12. Sensor outputs are used for scratch detection and roundness measurement of the ball. The sensor detects scratches with depths of 0.2 µm

or less and a few micrometres in width. The uncertainty of the roundness measurement is approximately 0.2 μm (peak to valley).

Fig 12.12 Automated surface measurement of artificial femoral head (left). Scratch detection and form measurement along the equator and across the pole of the ball are obtained. Measurement time of the surface is less than 10 s.

The measurement of form with scattered light may be achieved by a triangulation technique whereby the centre of mass of the measured angle distribution is detected and integrated along the scan direction. The sensitivity of the method as a function of surface spatial wavelength has been derived by Seewig et al. (2009).

As an example, a roundness measurement artefact with different sinusoidal waves was measured by Seewig et al.(2009). Fig. 12.13 shows the corresponding roundness profiles in polar coordinates. A reference measurement obtained with a tactile roundness gauge is shown on the left side. The reconstructed roundness profile obtained with the light scattering sensor is shown on the right side. The Pt (peak to valley) values differ by about 3 %.

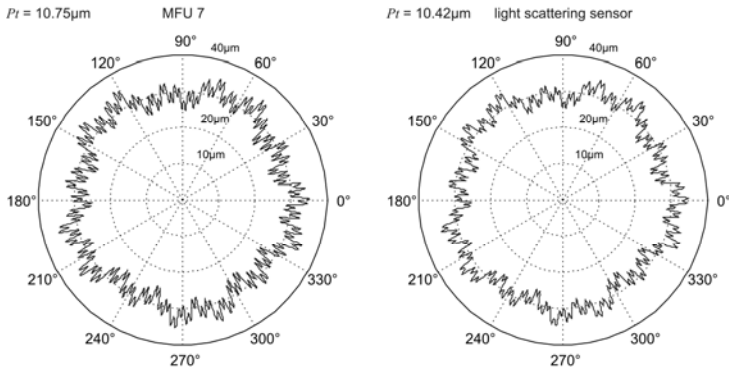

Fig 12.13 Left: tactile profile measurement of a roundness artefact with a *Pt* value of 10.75 µm. Right: reconstructed profile of the optical sensor data with a *Pt* value of 10.42 µm (Seewig et al. 2009)

As mentioned above, the surface roughness can be characterized by the parameter *Aq*, which is proportional to the second statistical moment, the variance, of the angle distribution. A mirror like surface has a small *Aq* value, and *Aq* increases depending on the RMS slope of the surface roughness. However, not only the roughness influences the *Aq* value. Any additional curvature caused by the workpiece form increases the value of the parameter. The influence of curvature can be suppressed using a correction term. For a cylindrical workpiece the correction term is proportional to $\left(D'/R_{zyl}\right)^2$, where D' is the diameter of the incident light spot and R_{zyl} is the radius of the cylinder. Correction terms for arbitrary form components can be calculated according to a mathematical formalism given by Seewig et al. (2009).

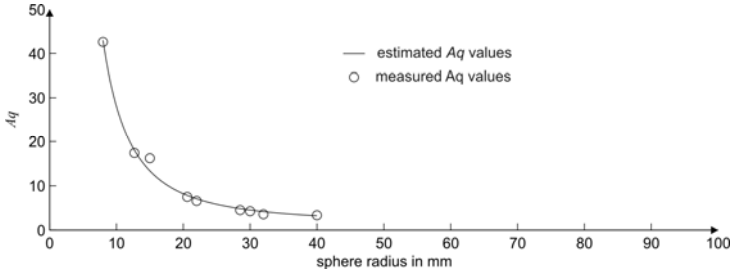

Fig 12.14 Estimated and measured *Aq* values for spheres with different radii but with the same micro structure

The influence of the workpiece curvature is shown in Fig. 12.14. Spheres with different radii but with the same micro-structure were measured. The circles indi-

cate Aq values of the sensor depending on the radii. The solid line is the estimated curve calculated from a priori knowledge about the workpiece form.

12.3.3 Recent developments in instrumentation for semiconductor manufacture (optical critical dimension)

Commercial optical scatterometers have been used for many years in semiconductor fabrication facilities and in hard disk manufacturing to monitor defects and particles on surfaces during manufacture. Some types are based on the use of TIS discussed in Sect. 12.2 (Schmitt Industries 2010). More recently, scatterometry has been widely used for monitoring and process control of the critical dimensions (linewidths) of semiconductor device features, even though that industry is producing features with 45 nm linewidth or smaller, and the pitch of lines is often smaller than the optical wavelengths of the scatterometers. With this measurement technology, called optical critical dimension (OCD) scatterometry, a reflectance signature of a number of nominally identical lines with a uniform pitch are measured together as a function of angle, wavelength, and/or polarization. The average linewidth and perhaps other average geometrical parameters are then calculated from least squares comparisons of the scattered light signatures with model simulations of the scattering.

Rigorous coupled wave (RCW) based theories are the most common methods used to analyze scatterometry data (Moharam et al. 1995, Li 1996). Simulations with different parameters are pre-calculated and stored in a library to facilitate rapid comparison with measured scattering data, or the data are fit to the model by regression analysis. Recent work has also focused on applying scatterometry to measure line sidewall angles as well as linewidth and to measure lines with even more complexity and thus more parameters. There are also efforts to use scatterometry for photomask CD metrology (Hoobler 2005, Pundaleva 2006). It is important to note, however, that scatterometry is used with gratings and is not well suited to measurement of individual features or non-periodic structures, although the individual grating elements can have complex shapes.

The accuracy of the OCD technique depends on at least three sets of factors: 1) realistic models for the geometrical structures of the surfaces being studied, 2) rigorous formulations for the electromagnetic scattering from the jagged, steeply sloped surface topography, and 3) a priori knowledge of the optical properties of the materials. Under these conditions it is often possible to calculate the average linewidth and other geometrical parameters of the fabricated features. Scatterometers are sometimes used in the so-called $\theta, 2\theta$ mode as shown in Fig. 12.15 (Raymond 2001) where the flux of the specular reflected beam is measured as a function of the angle of incidence. Although higher order diffracted intensities can also be measured when the pitch is sufficiently large, virtually every commercial instrument measures only the specular component. Moreover, because different

states of polarization produce different angle-resolved scattering signatures, separate scattering results are measured for *s*- and *p*-plane polarized light in the incident beam. While example measurements using the $\theta, 2\theta$ mode are discussed below, it is more common to measure either the specular reflectance (for example, Yang et al. 2004), or the polarization change upon reflection (for example, Niu et al. 2001), at a fixed angle as a function of optical wavelength to obtain the signature. The modeling procedure for these different data types is similar.

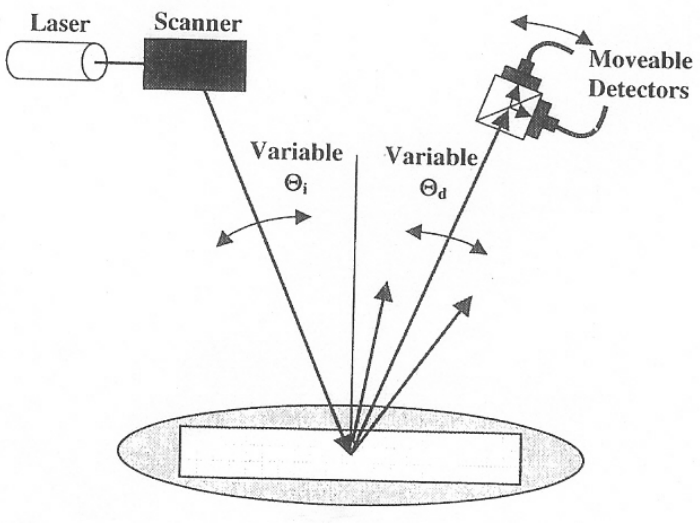

Fig. 12.15 Schematic diagram of a variable angle scatterometer useful for measuring the specular reflectance as a function of incident angle (Raymond 2001, reprinted with permission)

One example of research results obtained with OCD scatterometry is from Patrick et al. (2007) where scattering signatures were obtained for both *s*- and *p*-plane polarized light from linewidth targets fabricated on separation by implantation of oxygen (SIMOX) wafers. A model of the surface features is shown in Fig. 12.16. Silicon lines are fabricated over a buried silicon oxide (BOX) layer on a thin mixed boundary layer of silicon and silicon oxide, which is on a silicon wafer.

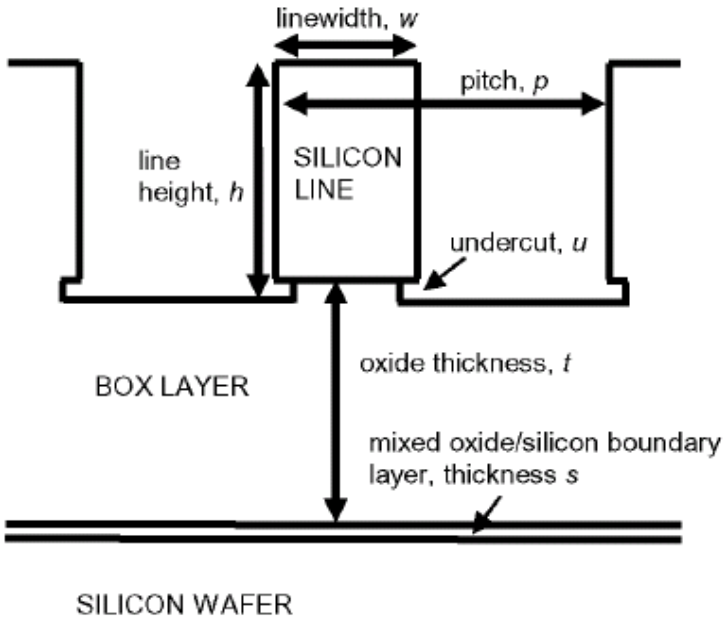

Fig. 12.16 Model of a patterned wafer surface used by Patrick et al. (2007) for OCD experiments. The model contains geometrical parameters, *w*, *h*, *p*, *u* (assumed to be the side of a square), *t*, *s*, and sidewall angle (assumed to be 90°), as well as the optical properties (real and imaginary) of silicon, the BOX layer, and the mixed layer

Many parameters were required for a complete description of the model in Fig. 12.16. The optical constants of the silicon substrate and the silicon lines were taken from the literature. The optical constants of the oxide and the thickness and composition of the mixed layer were taken from auxiliary scatterometry measurements from unpatterned wafers. The pitch was not fit but rather was considered to be well known a priori. The sidewall angle was assumed to be equal to 90° because of the single crystal nature of the silicon and its fabrication (Cresswell et al. 2006). The height of the silicon features was measured independently by AFM. The linewidth *w*, the undercut dimension *u* and the oxide thickness *t* were fitted by comparison to the model.

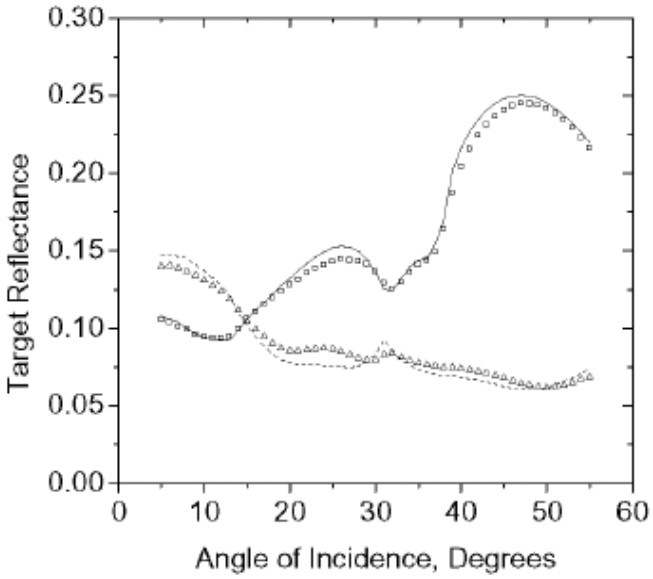

Fig. 12.17 Results (data points) obtained by Patrick et al. (2007) for specular reflectance of a patterned silicon surface as a function of angle compared with results (curves) calculated from the model of Fig. 12.16 with parameters yielding the best fit. The squares are for s-polarized incident light and the triangles are for *p*-polarized. The optical wavelength here was 532 nm, the pitch was 2.1 μm, and the best fit result for linewidth was 297.5 nm

One result for such a fit is shown in Fig. 12.17, where measured and modeled reflectances are plotted versus angle of incidence for *s*- and *p*-polarization. The fit of the model to the measurements is good, especially considering the number of factors that can influence the result. In this case the best fit linewidth was 297.5 nm.

Results for six different targets are shown in Fig. 12.18. Here the linewidths determined by OCD are compared to linewidths determined by scanning electron microscopy (SEM). While historically, top-down SEM and OCD measurements have often not been in perfect agreement, in this case the residuals from a fitted straight line are only a few nm. This agreement was likely aided by a priori knowledge of the 90° sidewall angle of the target.

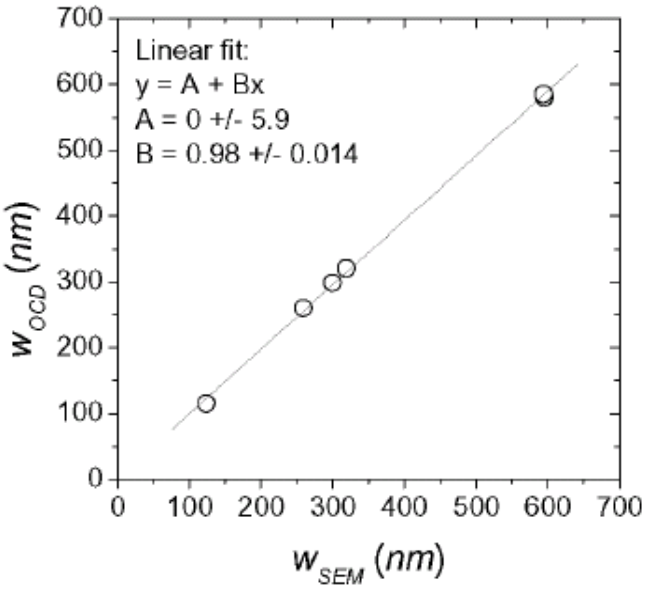

Fig. 12.18 Comparison of OCD results and SEM results for linewidth of six patterned structures (Patrick et al. 2007). The OCD results were obtained using the model of Fig. 12.16.

An emerging technique, known as scatterfield microscopy (Silver et al. 2007, Silver et al. 2009), combines elements of scatterometry and bright field imaging. The scatterfield technique uses a bright field microscope with structured incident light instead of a scatterometer. Measurements of the reflected light are taken at the conjugate back focal plane of the microscope objective where each point maps nominally to a plane wave of illumination at the sample. Microscope images of the patterned surfaces are acquired as a function of angle. The mean intensity of the angle-resolved images is calculated and then corrected using a background scan of the unpatterned surface that was previously normalized by the known silicon reflectance. This mode of operation is similar to conventional θ, 2θ scatterometry except that measurements are made with high magnification, image-forming optics. Scatterometry measurements throughout the field of view can be acquired in parallel by breaking the imaged field into an array of small targets or pixel groupings.

As above, the experimental signatures can be compared with simulations stored in a library of reflectance curves assembled from calculations performed for ranges of reasonably expected values of the parameters. A least-squares fitting routine is normally used to choose the optimum set of parameters that yields the closest experiment-to-theory agreement. When the parameter range is adequate and the

optical tools are accurately modeled, close agreement is achieved between the simulated and the measured curves, and nanometre scale agreement is obtained between the best-fit parameters and known values. Correlations between parameters, measurement noise, and model inaccuracies all lead to measurement uncertainty in the fitting process.

An example of scatterfield data (Silver et al. 2009) from a grating of dense, sub-wavelength features in the 120 nm size range is shown in Fig. 12.19. Strong sensitivity to changes in sidewall angles as well as to critical dimensions below the conventional imaging resolution limits can be observed using this type of optical method. Good agreement between the simulated reflectance curves and the experimental data is also achieved.

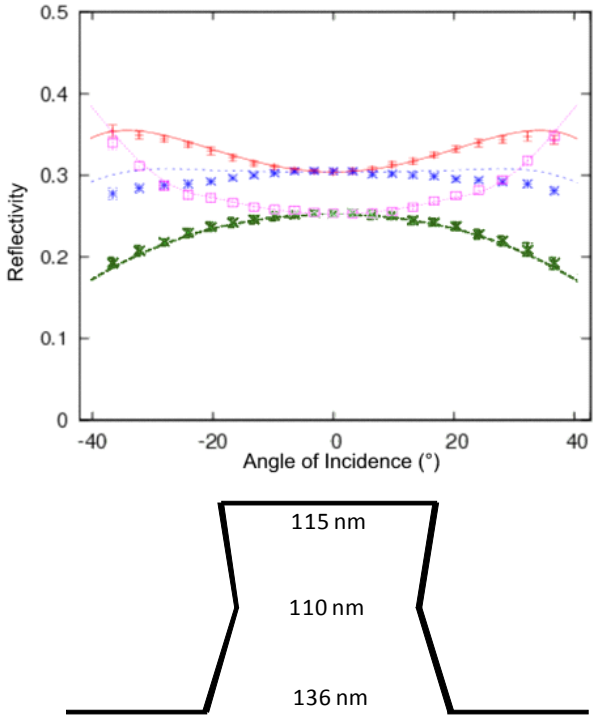

Fig. 12.19 An example of experimental data points and library data fits (top) for a periodic silicon test structure (bottom). The pitch of the features was 300 nm and the optical wavelength was 450 nm. Three parameters are required to characterize the line shape in order to obtain a good fit between the data points and simulated curves. The four sets of data represent angle scans with *s*- and *p*-polarization taken in both the *x* and *y* directions. Good agreement with reference values was obtained for the top and middle width parameters

An example of fitting scatterfield data for linewidth features in the 40 nm to 60 nm sized range is shown in Tab. 12.1 (Silver et al. 2009). These data are parametric fitting results for dense features fabricated in silicon using a standard front end semiconductor manufacturing process. The nominal ratio of pitch to width was 3:1. Tab. 12.1 shows results obtained from different techniques for comparison. This is an example of how accurate optical metrology can be performed if the data are accurately normalized and the parametric fits take account of the proper floating parameters.

Tab. 12.1 Results obtained for height (*h*) and width (*CD*) parameters of dense linewidth features. The optical wavelength used for the scatterfield (OCD) results was 450 nm. The OCD results and small angle x-ray scattering (SAXS) results use parametric fits to a stacked trapezoid model similar to the one illustrated in Fig. 12.19. The agreement between techniques is especially good for the top and middle *CD*s. Top-down SEM used here is not sensitive to line height

Method	CD_{TOP}	CD_{MID}	CD_{BOT}	h
	/nm	/nm	/nm	/nm
OCD	41	49	63	56
AFM	38	45	50	55
SAXS	43	53	62	54
SEM	35	49	63	-

12.4 Instrument use and good practice

Good practice for the specification and measurement of scattered light from rough surfaces may be found in several documentary standards and guidelines developed by different organizations, including the ASTM, SEMI, and the ISO. Some of these standards are discussed below.

12.4.1 SEMI MF 1048-1109 (2009) Test method for measuring the effective surface roughness of optical components by total integrated scattering

SEMI MF 1048-1109 (2009) succinctly describes the apparatus, physical standards, measurement procedure, analysis and quality control procedure recommended for a measurement of TIS. A schematic diagram of the apparatus reproduced from the standard is shown in Fig. 12.20. The main feature is a Coblentz sphere, which focuses the scattered light to a single detector but which contains an aper-

ture to allow the specular beam to pass through. The recommended design involves trade-offs. Since it is difficult to measure scattered light right up to the specular beam and right out to grazing, the standard specifies a sphere with a minimum collecting angle of 70° with respect to the sample normal and an aperture that subtends 5° or less at the specimen. Therefore, a portion of the scattered light is not detected. Within these measurement limits, the effective surface roughness is calculated from equation (12.5). The document also specifies the use of physical standards for both diffuse reflectance and specular reflectance in the TIS measurement process to ensure the calibration of the TIS results.

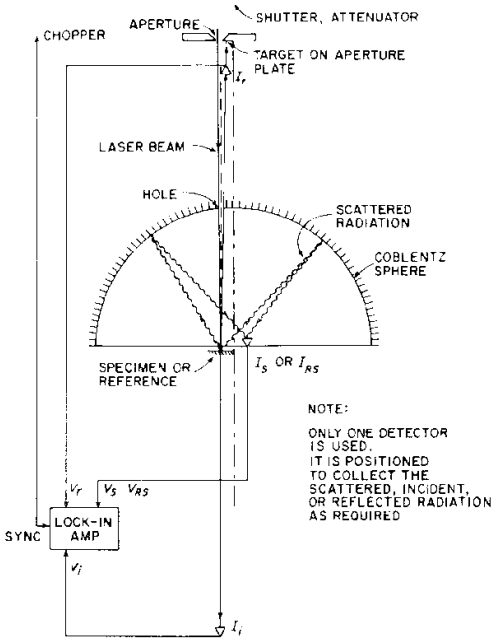

Fig. 12.20 Schematic diagram of a TIS apparatus (SEMI MF 2009, reprinted with permission from Semiconductor Equipment and Materials International, Inc. (SEMI) © 2010)

12.4.2 SEMI ME1392-1109 (2009) Guide for angle resolved optical scatter measurements on specular or diffuse surfaces.

SEMI ME 1392-1109 (2009) describes procedures for measuring BRDF with a scattered light apparatus. The BRDF is defined as

$$\mathrm{BRDF} = P_r /(P_i \, d\omega_r \cos\theta_r), \tag{12.11}$$

and is the standard approach for describing scattered light in radiometry (Nicodemus et al. 1977). A schematic diagram of the quantities appearing in equation (12.11) is shown in Fig. 12.21. An attachment to the standard, termed "Related Information," also describes briefly how the surface RMS roughness and PSD may be calculated from the measured BRDF through a scatter model. The RMS roughness is calculated from the TIS, which is obtained in turn by integrating the BRDF function over the angles of the scattered light; the PSD function may be calculated directly from the BRDF itself.

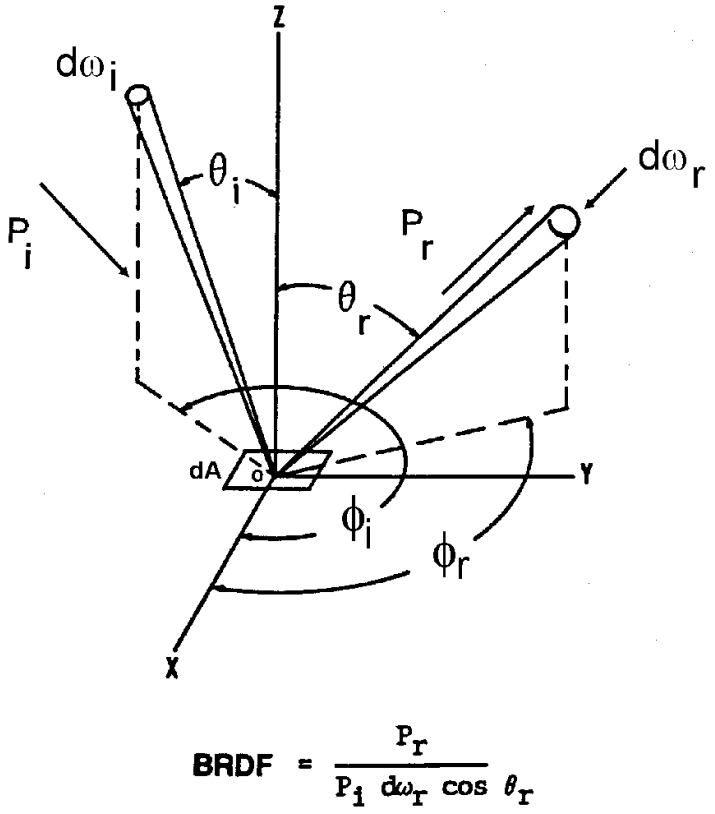

Fig. 12.21 Schematic diagram of the BRDF concept to describe light scattered from a rough surface (Nicodemus 1977). See also SEMI ME (2009)

12.4.3 ISO10110-8: 2010 Optics and photonics — Preparation of drawings for optical elements and systems — Part 8: Surface texture

Without describing mathematical details, ISO 10110-8 (2010b) characterizes the close relationship between the surface roughness and the light scattering properties of optical surfaces and describes drawing indications that one can use to specify RMS roughness, RMS slope and power spectral density for an optical surface. It is assumed here that these parameters for characterizing surface quality are derived from line profiling measurements. The standard uses a model with two parameters, A and B, to represent the PSD

$$\mathrm{PSD}(f) = A / f^{B}, \tag{12.12}$$

between spatial frequency limits characterized by two more parameters, C and D. Fig. 12.22 taken from an informative annex of the standard, shows example values of the parameters for several different levels of optical finish.

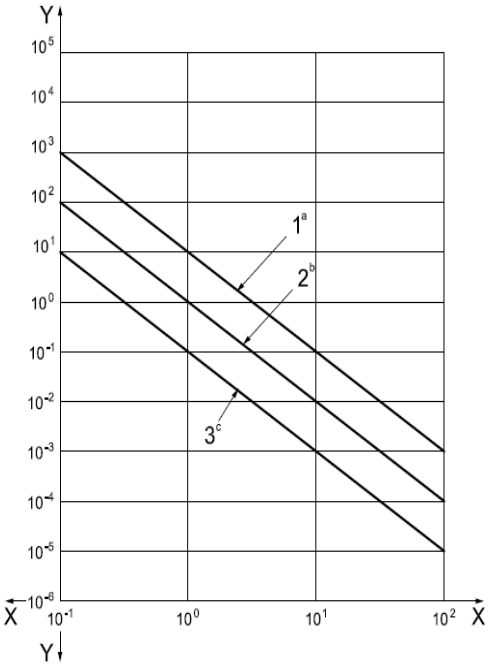

Key

X spatial frequency, in mm^{-1}
Y power spectral density, $nm^2 \times mm$
1 ordinary polish PSD
2 precision polish PSD
3 super polish PSD

[a] $A = 10\ nm^2 \times mm^{-1}$
[b] $A = 1\ nm^2 \times mm^{-1}$
[c] $A = 0{,}1\ nm^2 \times mm^{-1}$

Fig. 12.22 Examples of three power spectral density specifications modeled with the formula PSD(f) = A/f^2, (ISO 2010b, reprinted with permission). The lines represent different levels of polish of the surface, and the parameter A is shown for each line. The PSD has the units of [nm^2 mm] here.

12.4.4 Standards for gloss measurement

Standards ASTM D523 – 08, *Standard Test Method for Specular Gloss* (ASTM 2008), and ISO 2813: 1994, *Paints and varnishes -- Determination of specular gloss of non-metallic paint films at 20 degrees, 60 degrees and 85 degrees* (ISO 1994), are two of several standards written to describe the measurement of specular gloss, a property related to roughness that is important to the appearance and function of products. The standards describe similar specifications for gloss meas-

uring instruments. In particular they specify identical choices for the angle of incidence—20°, 60,° and 85°—along with the angular sizes of the apertures for each angle of incidence. Fig. 12.23, taken from ASTM D523, shows a typical gloss measurement configuration and is very similar to a comparable figure in ISO 2813.

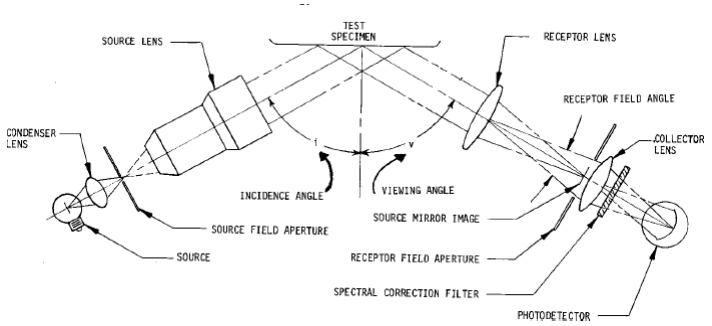

Fig. 12.23 Diagram of parallel-beam glossmeter showing apertures and the source mirror-image position, reprinted, with permission, from ASTM D523-08 Standard Test Method for Specular Gloss, copyright ASTM International, 100 Barr Harbor Drive, West Conshohocken, PA 19428.

12.4.5 VDA Guideline 2009, Geometrische Produktspezifikation Oberflächenbeschaffenheit Winkelaufgelöste Streulichtmesstechnik Definition, Kenngrößen und Anwendung (Light Scattering Measurement Technique)

VDA Guideline 2009 from the German automotive association (VDA 2009) refers to the light scattering method specifically used by scatterometers similar to the design shown in Fig. 12.9. The guideline provides information on the measurement principle (Fig. 12.24 top)—normal incidence areal LED-illumination of the surface and collection of the scattered light by a linear diode array in a given angle range (for example ± 16°). The guideline also indicates the use of statistical parameters *Aq* (variance), *Ask* (skewness) and *Aku* (kurtosis) of the scattered light angle distribution for roughness characterization and describes rules for indicating those parameters in technical drawings (Fig. 12.24 bottom).

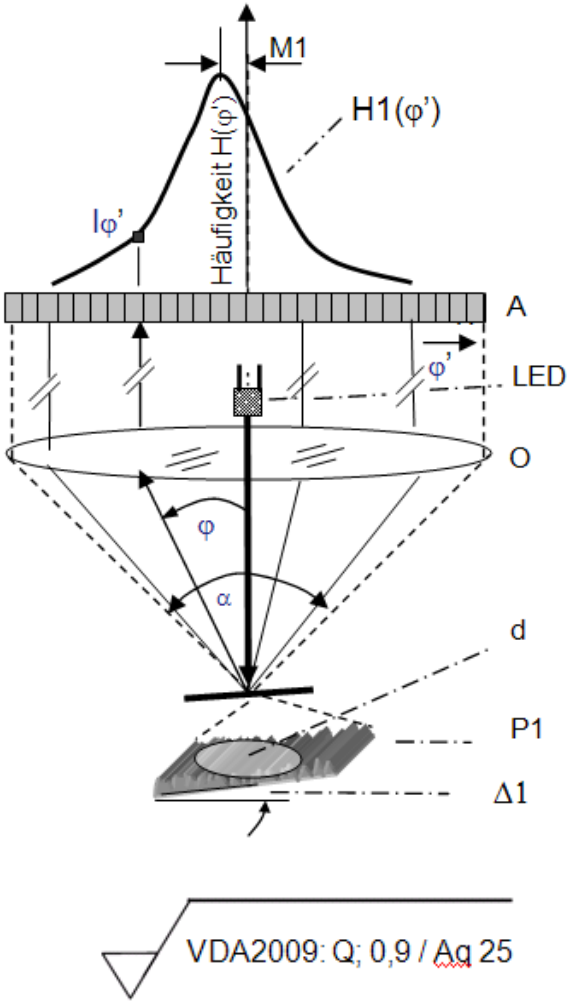

Fig. 12.24 Scatterometer schematic (top) and example (bottom) of drawing notation described in the VDA 2009 guideline, reprinted with permission. The term "Häufigkeit" means "light intensity" here.

12.5 Limitations of the technique

The phenomenon of light scattering has suggested the promise of assessing rapidly a great deal of information about surface topography because, in principle, all of the information about the surface topography is contained in the pattern of scattered light. However, there are both theoretical and experimental limitations to this suggestion. On the theoretical side, the assessment of surface texture geometry parameters from measured scattering quantities is based on models—valid, useful models, but models all the same. The RMS roughness (*Rq* or *Sq*) calculated from a model using scattered light measurements is not identical to the *Rq* or *Sq* value calculated from a profile or a topography image. This is principally due to the difficulty of matching the bandwidth limits of the two methods. In addition, the useful relationships in equations (12.2) to (12.9) for assessing surface texture parameters from scattered light are approximations that are only valid over certain limits, such as very smooth surfaces or surfaces with modest slopes or surfaces with Gaussian height distributions. When shadowing or multiple scattering effects need to be accounted for, assessing surface texture parameters becomes much more complicated.

Experimentally, the dynamic range of light scattering instruments is often more limited than profiling instruments. If a single multi-element camera is used for measuring the light intensity over different channels or directions, the dynamic range of measurable intensities can be limited. Special techniques would then be required to attenuate the stronger parts of the scattered light with respect to the weaker parts, in order to avoid saturation of some of the detector elements and to maintain signal-to-noise in other detector elements. In addition, the range of measured spatial wavelengths is limited by the ability to separate the specularly reflected light from the scattered light. If an angle resolved detection system has a range of ± 20° and the light source is normally incident with a wavelength of 500 nm and produces a specular beam with a width of 2° on the detection system, the range of measurable spatial wavelengths is only about 1.5 μm to 14 μm. A very good angular resolution and a wide dynamic range of flux sensitivity are required to assess quantitatively a wide range of spatial wavelengths and amplitudes.

12.6 Extensions of the basic principles

We have emphasized the metrological usefulness of only three properties of light scattered by rough surfaces: the specular beam intensity, the integrated light scatter and the angle resolved light scatter. Other properties have also been widely studied for assessing surface roughness. These include 1) various aspects of laser speckle (Asakura 1978), 2) polarization changes upon reflection, which can be assessed with ellipsometry (Azzam and Bashara 1977, Niu et al. 2001), and 3) the

phenomenon of enhanced backscatter (O'Donnell and Mendez 1987) characterized both experimentally and theoretically (for example Maradudin et al. 1990). One of O'Donnell and Mendez's results is shown in Fig. 12.25. The specular-like enhanced backscatter peak was experimentally separated from the incident light by a partially reflecting folding mirror positioned along the incident light path.

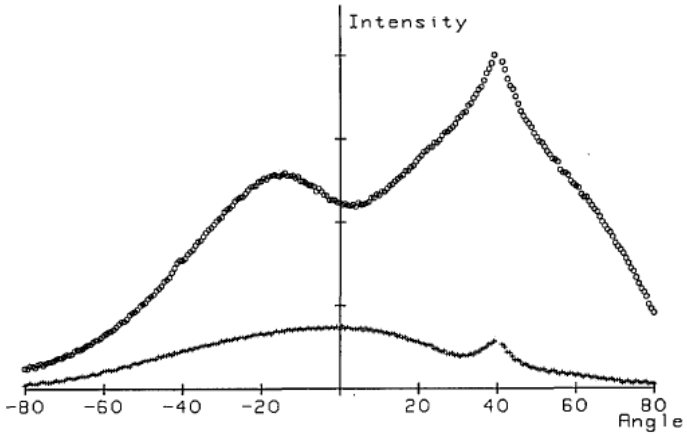

Fig. 12.25 Early observation of enhanced backscatter from a reflecting metal surface (O'Donnell and Mendez 1987, reprinted with permission). The angle of incidence was 40° from the right and the backscatter direction is +40.° The upper graph shows the scattering of *s*-polarized light for incident light that is also *s*-polarized. The lower curve shows the scattering for cross polarization, that is, the incident light is *s*-polarized and the scattered light is *p*-polarized

Studies of solid surfaces using techniques employing visible or near visible light have also been discussed. There is besides a huge body of work involving microwave, ultrasonic, and radar sources for various applications such as the practical studies of ground, water, and atmospheric surfaces over large distance scales, as well as the earth as a whole, the moon, and other planets (Beckmann and Spizzichino 1987).

12.7 Acknowledgements

The authors would like to thank Mr. J Glenn Valliant of Schmitt Industries, Dr. John Stover of the Scatterworks, Dr. Kevin O'Donnell of the CICESE, and Dr. Bryan Barnes, Dr. Hui Zhou, Dr. Ravi Attota, Mr. Michael Stocker, Dr. Egon

Marx, Dr. Thomas Germer, and Dr. Heather Patrick of NIST for technical contributions to this chapter.

12.8 References

Asakura T (1978) Surface roughness measurement. In Dainty J C, Speckle metrology. Academic Press

ASTM (2008) D 523 – 08: Standard test method for specular gloss. ASTM International

Azzam R M A, Bashara N M (1977) Ellipsometry and polarized light. North Holland

Beckmann P, Spizzichino A (1987) The scattering of electromagnetic waves from rough surfaces. Artech House, Inc.

Bennett H E, Porteus J O (1961) Relation between surface roughness and specular reflectance at normal incidence. J Opt Soc Am 51:123-129

Bennett J M, Mattsson L (1989) Introduction to surface roughness and scattering. Optical Society of America. Sections 3.C.1, 4.E, and 4.F

Brodmann B, Brodmann R, Bodschwinna H, Seewig J (2009) Theory and measurements of a new light scattering sensor. Proceedings 12th Int. Conf. on Metrology and Properties of Engineering Surfaces. Rzeszow, Poland

Brodmann R, Gerstorfer O, Thurn G (1985) Optical roughness measurement for fine machined surfaces. Opt Eng 24:408-413

Brodmann R, Allgäuer M (1988) Comparison of light scattering from rough surfaces with optical and mechanical profilometry in Surface Measurement and Characterization. Proc SPIE 1009:111-118

Cao L X, Vorburger T V, Lieberman A G, Lettieri T R (1991) Light-scattering measurement of the rms slopes of rough surfaces. Appl Opt 30:3221-3227

Chandley P J (1976) Determination of the autocorrelation function of height on a rough surface from coherent light scattering. Opt Quantum Electron 8:329-333

Church E L (1979) The measurement of surface texture and topography by differential light scattering. Wear 57:93-105

Church E L, Jenkinson H A, Zavada J M (1979) Relationship between surface scattering and microtopographic features. Opt Eng 18:125-136

Cresswell M W, Guthrie W F, Dixson R G, Allen R A, Murabito C E, Martinez de Pinillos J (2006) RM 8111: Development of a prototype linewidth standard. J Res. NIST 111:187- 203

Davies H (1954) The reflection of electromagnetic waves from a rough surface. Proc Inst Elec Engrs 101: 209-214

Elson J M, Bennett J M (1979) Relation between the angular dependence of scattering and the statistical properties of optical surfaces. J Opt Soc Am 14:1788-1795

Flinn G (accessed, April 21, 2010) How Mirrors Work, http://science.howstuffworks.com/mirror.htm/printable

Germer T A, Asmail C C (1997) A goniometric optical scatter instrument for bideirectional reflectance distribution function measurements with out-of-plane and polarimetry capabilities. Proc SPIE 3141:220-231

Griffiths B J, Middleton R H, Wilkie B A (1994) Light scattering for the measurement of surface finish: a review. Int J Prod Res 32:2683-2694

Hoobler R J (2005) Optical critical dimension metrology, in Rizvi S, ed. Handbook of photomask manufacturing technology. CRC Press, Boca Raton

ISO (1994) 2813: Paints and varnishes - Determination of specular gloss of non-metallic paint films at 20 degrees, 60 degrees and 85 degrees. International Organization for Standardization

ISO (1996) 13565-1: Geometrical Product Specifications (GPS) -- Surface texture: Profile method; Surfaces having stratified functional properties -- Part 1: Filtering and general measurement conditions. International Organization for Standardization

ISO (2010a) 25178-6: Geometrical product specifications (GPS) — Surface texture: Areal — Part 6: Classification of methods for measuring surface texture. International Organization for Standardization

ISO (2010b) 10110-8: Optics and photonics — Preparation of drawings for optical elements and systems — Part 8: Surface texture. International Organization for Standardization

Kiely A B, Lettieri T R, Vorburger T V (1992) A model of an optical roughness-measuring instrument. Int. J. Mach. Tools Manuf. 32: 33-35

Li L (1996) Use of Fourier series in the analysis of discontinuous periodic structures. J Opt Soc Am A 13: 1870-1876

Maradudin A A, Michel T, McGurn A R, Méndez E R (1990) Enhanced backscattering of light from a random grating. Ann Phys 203 (2): 255-307

Marx E, Vorburger T V (1990) Direct and inverse problems for light scattering by rough surfaces. Appl Opt 29:3613-3626

Marx E, Leridon B, Lettieri T R, Song J-F, Vorburger T V (1993) Autocorrelation functions from optical scattering for one-dimensionally rough surfaces. Appl Opt 32: 67- 76

Moharam M G, Grann E B, Pommet D A, Gaylord T K (1995) Formulation for stable and efficient implementation of the rigorous coupled-wave analysis of binary gratings. J Opt Soc Am A 12: 1068-1076

Moharam M G, Pommet D A, Grann E B, Gaylord T K (1995) Stable implementation of the rigorous coupled-wave analysis for surface-relief gratings: enhanced transmittance matrix approach. J Opt Soc Am A 12: 1077-1086

Nadal M E, Thompson E A (2000) New primary standard for specular gloss measurements. J Coatings Technol 72:61-66

Nicodemus F E, Richmond J C, Hsia J J, Ginsberg I, Limperis T (1977) Geometrical considerations and nomenclature for reflectance, NBS Monograph No. 160. U.S. Dept. of Commerce, Washington

Niu X, Jakatdar N, Bao J, Spanos C J (2001) Specular Spectroscopic Scatterometry. IEEE Trans Semicond Manuf 14: 97-111

O'Donnell K A, Mendez E R (1987) Experimental study of scattering from characterized random surfaces. J Opt Soc Am A 4:1195-1205

Optosurf (2010a) www.optosurf.com. revised (2010). accessed (Sept. 24, 2010)

Optosurf (2010b) www.optosurf.de/images/stories/Datenblaetter /Applikationsdatenblatt_12_10_10_Kurbelwelle.pdf. accessed (Nov. 19, 2010)

Patrick H J, Germer T A, Cresswell M W, Allen R A, Dixson R G, Bishop M (2007) Modeling and analysis of scatterometry signatures for optical critical dimension reference material applications, in CP931, Frontiers of Characterization and Metrology for Nanoelectronics, ed. Seiler DG et al. American Inst. of Physics

Pundaleva I, Chalykh R, Kim H, Kim B, Cho H (2007) Scatterometry based profile metrology of two-dimensional patterns of EUV masks. Proc SPIE 6607:66070S

Rakels J H (1989) Recognized surface finish parameters obtained from diffraction patterns of rough surfaces. Proc SPIE 1009:119-125

Raymond C J (2001) Scatterometry for semiconductor metrology, Chapter 18 in Handbook of Silicon Semiconductor Metrology Diebold AC, ed. Marcel Dekker

Schmitt Industries (2010) http://www.schmitt-ind.com/sms.html. accessed (Sept. 24, 2010) .

Seewig J, Beichert G, Brodmann R, Bodschwinna H, Wendel M (2009) Extraction of shape and roughness using scattered light. Proc. SPIE 7389: 73890N

SEMI ME 1392-1109 (2009) Guide for angle resolved optical scatter measurements on specular or diffuse surfaces. Semiconductor Equipment and Materials International

SEMI MF 1048-1109 (2009) Test method for measuring the effective surface roughness of optical components by total integrated scattering. Semiconductor Equipment and Materials International

Silver R M, Barnes B, Attota R, Jun J, Stocker M, Marx E Patrick H (2007) Scatterfield microscopy to extend the limits of image-based optical metrology. Appl. Opt. 46: 4248-4257

Silver R M, Zhang N F, Barnes B M, Zhou H, Heckert A, Dixson R, Germer T A, Bunday B (2009) Improving optical measurement accuracy using multi-technique nested uncertainties. Proc. SPIE 7272:727202

Stover J C (1988) Optical scatter. Lasers and Optronics. 7(7)

Stover J C (1995) Optical scattering measurement and analysis. 2nd edn. SPIE Optical Engineering Press

Valliant J G, Foley M P, Bennett J M (2000) Instrument for on-line monitoring of surface roughness of machined surfaces. Opt. Eng. 39: 3247 – 3254

VDA 2009 (2009) Geometrische Produktspezifikation Oberflächenbeschaffenheit Winkelaufgelöste Streulichtmesstech-nik Definition, Kenngrößen und Anwendung (Light Scattering Measurement Technique). Verband der Automobilindustrie E.V., Frankfurt

Vorburger T V, Marx E, Lettieri T R (1993) Regimes of surface roughness measurable with light scattering. Appl. Opt. 32: 3401-3408

Vorburger T V, Rhee H G, Renegar T B, Song J F, Zheng A (2007) Comparison of optical and stylus methods for measurement of rough surfaces. Int. J. Adv. Manuf. Technol. 33: 110-118; DOI 10.1007/s00170-007-0953-8

Yang W, Hu J, Lowe-Webb R, Korlahalli R, Shivaprasad D, Sasano H, Liu W, Mui D S L (2004) Line-Profile and Critical-Dimension Monitoring Using a Normal Incidence Optical CD Metrology. IEEE Trans Semicond Manuf 17: 564-572

Zimmerman J H, Vorburger, T V Moncarz H T (1988) Automated optical roughness inspection. Proc SPIE 954: 252-264